Italian Journal of Engineering Geology and Environment
www.ijege.uniroma1.it

ANALYZING URBANIZATION AND ENVIRONMENTAL CHANGE IN AÏN FAKROUN, ALGERIA USING LANDSAT IMAGERY THROUGH GOOGLE EARTH ENGINE

Maya BENOUMELDJADJ[(*)], Samir BOUGHOUAS[(**)],
Malika RACHED-KANOUNI[(***)] & Abdelouahab BOUCHAREB[(****)]

[(*)]Larbi Ben Mhidi University - Oum El Bouaghi (Algeria) and Salah Boubnider University of Constantine 3, Earth Sciences and Architecture Faculty, Department of Architecture, AUTES Research Laboratory - Constantine (Algeria)
[(**)]Salah Boubnider University of Constantine 3, Faculty of Architecture - Constantine (Algeria)
[(***)] Larbi Ben Mhidi University - Oum El Bouaghi (Algeria) and Salah Boubnider University of Constantine 3, AUTES Research Laboratory - Constantine (Algeria)
[(****)]Salah Boubnider University of Constantine 3, AUTES Research Laboratory - Constantine (Algeria)
Corresponding author: maya.benoumeldjadj@univ-oeb.dz

EXTENDED ABSTRACT

Questo studio esamina le dinamiche spazio-temporali dell'uso e della copertura del suolo e la loro relazione con le variazioni climatiche locali, tra cui la temperatura superficiale del terreno, l'indice di vegetazione a differenza normalizzata (NDVI) e l'indice di edificio a differenza normalizzata (NDBI), nel comune di Aïn Fakroun in Algeria, zona semi-arida, su un periodo di 30 anni, dal 1993 al 2023, dal 1° gennaio al 31 dicembre.

L'analisi si basa sull'utilizzo di immagini satellitari LANDSAT/LT05/C02/T1_L2 per l'anno 1993 e LANDSAT/LC08/C02/T1_L2 per l'anno 2023. Queste immagini sono state elaborate tramite la piattaforma *Google Earth Engine*, caratterizzata da un'elevata potenza di elaborazione geospaziale che consente l'accesso a dati multitemporali e calcoli avanzati senza il *download* diretto delle immagini, applicando un classificatore Random Forest (RF) e lavorando con le seguenti classi: area urbana, terreno nudo, vegetazione e foresta.

L'obiettivo di questa ricerca è comprendere come le trasformazioni dell'uso del suolo siano legate alle variazioni termiche della superficie terrestre, in un contesto regionale caratterizzato da una rapida urbanizzazione e da una crescente pressione sulle risorse naturali. Questo è parte di un approccio analitico volto a supportare le politiche di pianificazione territoriale integrando dati oggettivi provenienti da telerilevamento.

I dati elaborati hanno permesso di mappare le principali tipologie di uso del suolo e di analizzarne i cambiamenti nell'arco di tre decenni. Questo approccio è stato abbinato all'estrazione della temperatura superficiale del suolo (LST), utilizzata come indicatore chiave per valutare l'impatto dei cambiamenti di uso del suolo sulle variazioni termiche locali. L'indice NDVI è stato utilizzato per quantificare le dinamiche della vegetazione, mentre l'indice NDBI è stato utilizzato per monitorare l'espansione urbana e il suo contributo all'effetto isola di calore urbano. Lo studio mostra una notevole evoluzione nella struttura del paesaggio: le aree urbanizzate hanno registrato un progressivo aumento (+2%), a scapito delle superfici nude (dal 94% al 43%), mentre la copertura vegetale è leggermente aumentata grazie alle iniziative agricole e forestali programmate dallo Stato algerino, come la riforestazione nell'ambito del programma internazionale "Algeria Verde". Parallelamente, l'analisi delle tendenze termiche indica un aumento significativo della temperatura massima superficiale, un fattore climatico importante per comprendere la relazione tra la superficie terrestre e l'atmosfera. Passando da 41.54 °C nel 1993 a 46.66 °C nel 2023, si è registrato un accentuato riscaldamento regionale nelle aree densamente edificate, principalmente legato alla realizzazione di progetti residenziali, infrastrutture industriali e progetti stradali nel nord del comune. La correlazione negativa tra NDVI e LST conferma il ruolo moderatore delle superfici vegetate sul microclima locale, mentre la correlazione positiva tra NDVI e LST evidenzia l'effetto esacerbato dei materiali urbani impermeabili sull'aumento delle temperature. Questi risultati evidenziano l'interconnessione tra uso del suolo, uso del suolo e dinamiche climatiche locali, sottolineando al contempo l'importanza di integrare questi parametri nelle future politiche di sviluppo.

L'urbanizzazione rapida e non pianificata, concentrata principalmente nel centro e nel sud della regione, è stata identificata come un fattore importante in questo aumento della temperatura. Sebbene parte del territorio abbia beneficiato di misure di riforestazione o dell'espansione dei terreni agricoli, questi sforzi rimangono insufficienti a compensare l'aumento delle aree edificate.

In conclusione, questa ricerca evidenzia l'importanza di monitorare le tendenze del cambiamento dell'uso del suolo per comprendere meglio gli impatti locali dello sviluppo urbano e offre ai responsabili politici percorsi concreti per promuovere una pianificazione urbana sostenibile, come l'integrazione di infrastrutture verdi, l'uso di materiali ad alto albedo e la pianificazione integrata di nuovi quartieri. Queste misure mirano a mitigare gli effetti termici dell'urbanizzazione e a rafforzare la resilienza climatica di Aïn Fakroun nel contesto semi-arido algerino. Infine, i risultati sono importanti per comprendere meglio le modalità di gestione sostenibile delle risorse naturali nelle regioni aride e semi-aride, nonché i metodi efficaci per studiare questi processi.

IJEGE, 1 (2025): 31-42, DOI: 10.4408/IJEGE.2025-01.O-05
E-ISSN 2035-5688 | ISSN 1825-6635 / ©Author(s)

ABSTRACT

This study examines the spatiotemporal dynamics of land use and land cover, as well as their relationships with surface temperature, normalized difference vegetation index, and normalized difference building index, in Aïn Fakroun, Algeria, over 30 years from January 1 to December 31 of the years 1993 and 2023. Using advanced remote sensing tools and the Google Earth Engine platform, Landsat-5 imagery for the year 1993 and Landsat-8 for the year 2023 were analyzed to examine significant environmental and urban transformations induced by climate change and rapid urbanization. The main findings reveal a marked increase in urban areas (nearly 2%) and vegetation, accompanied by a reduction in bare land, from 94% to 43%. However, this growth has exacerbated the urban heat island effect, with Land Surface Temperature values increasing across all land cover categories. For example, the maximum land surface temperature increased from 41.54°C in 1993 to 46.66°C in 2023, indicating substantial regional warming.

The study found an inverse relationship between the Normalized Difference Vegetation Index and land surface temperature, with vegetated areas exhibiting lower surface temperatures. A positive correlation between the Normalized Difference Vegetation Index (NDVI) and land surface temperature highlights the thermal effects of urbanization. Urban areas have expanded significantly, particularly in the center and south of the region, while vegetation and forest cover have increased slightly in the north. These changes suggest a landscape transformation shaped by urban growth and reforestation efforts.

The results provide policymakers with actionable information, advocating for sustainable practices such as integrating green infrastructure and high-albedo materials to mitigate urban heat island effects and enhance resilience to climate change. This research contributes to the understanding of the interaction between urbanization, vegetation, and surface temperature and offers recommendations for sustainable urban planning in Aïn Fakroun.

Keywords*: urban heat island, land use/land cover, Google Earth Engine (GEE), climate change, sustainable urban planning*

INTRODUCTION

Rising urban temperatures are attributed to the reduction of green spaces and water surfaces in favor of impermeable materials, such as concrete and asphalt, which are characterized by low albedo and high thermal inertia (Voogt & Oke, 2003). Added to this are human activities such as transport, industry, and the intensive use of air conditioning. These factors accentuate the urban heat island (UHI) effect by modifying local heat exchanges, which directly affects the urban microclimate (Azevedo *et alii*, 2016).

Thermal impacts, combined with evaporation, drought, and erratic precipitation, highlight the significant temperature variability in this area (Sultan, 2011). Geographic information systems (GIS) and remote sensing are crucial in addressing the challenges posed by global warming. These tools enable the development of new land-cover classification algorithms, the processing of large volumes of data, and the integration of thermal calculation methods (Zeren Cetin *et alii*, 2023). The advent of Google Earth Engine (GEE), a revolutionary cloud platform dedicated to geospatial analysis, has significantly transformed the access and processing of high-resolution satellite imagery, greatly facilitating large-scale environmental monitoring (Gorelick, 2013).

Using GEE, it is now possible to accurately calculate surface temperature (LST) (Vinh *et alii*, 2020), as well as indices such as the Normalized Difference Vegetation Index (NDVI) to assess vegetation density and health and the Normalized Difference Building Index (NDBI) to monitor urbanization (Kumar & Shekhar, 2015).

The parameters (LST) and NDVI) have become essential for understanding climate trends, assessing environmental changes, and monitoring vegetation trends at regional and global scales (Vinh *et alii*, 2020). At the same time, NDBI has emerged as a valuable tool for quantifying the degree of urbanization of territories (Malik *et alii*, 2019). Recent studies have revealed significant correlations between these environmental indicators (Guha & Govil, 2022). The intensification of urbanization is systematically accompanied by an increase in surface temperature, which is reflected in a positive correlation between NDBI and LST, highlighting the thermal impact of urban development (Mahcer *et alii*, 2024). Conversely, areas characterized by dense and abundant vegetation have significantly lower surface temperatures (Marzban *et alii*, 2018). The acceleration of the urbanization process leads to dynamic changes in land use and cover, as well as higher LST values (Budhwar *et alii*, 2023). A new indicator, the Vegetation Health Index (VHI), enriches this analysis by providing a more accurate assessment of the impact of droughts on vegetation (Benoumeldjadj *et alii*, 2024).

Understanding and monitoring land use and cover changes (LUCCs) have become essential for effective urban planning and sustainable environmental management (Patel *et alii*, 2023).

Recent studies have highlighted complex interactions between three key parameters: land use change, land surface temperature (LST), and various soil indices (Paz-Ferreiro & Fu, 2016).

The present study focuses on assessing the interrelationships among LST, NDVI, NDBI, LULUCF, and land cover changes using multispectral Landsat images (USGS.gov, 2019) for the years 1993 and 2023. Thus, regions particularly vulnerable to drought are identified using GIS tools and NDVI-VHI indices (Singh *et alii*, 2015; Zellweger *et alii*, 2019).

MATERIALS AND METHODS

Study area

The study focuses on the commune of Aïn Fakroun, located northeast of the city of Oum El Bouaghi in Algeria (Fig. 1). It is situated between 35.90°N and 36.05°N in latitude and 6.70°E and 6.90°E in longitude, covering an area of approximately 262 km². Located at the interface between arid and semi-arid climates, the region is sensitive to the impacts of climate change (Sultan, 2011). A mixture of plains and low hills characterizes the city's topography, with altitudes ranging from 800 to 1200 meters above sea level.

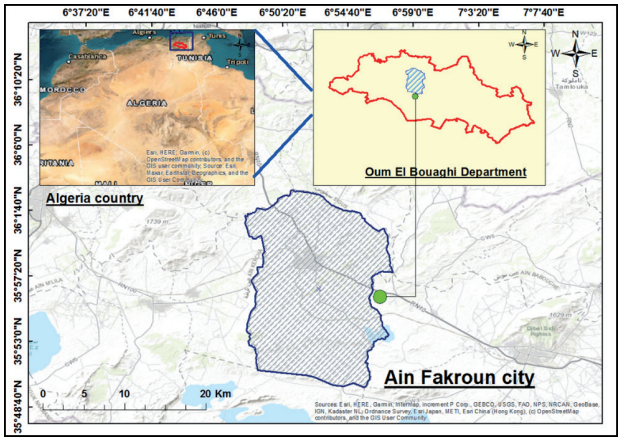

Fig. 1 - Location of Ain Fakroun

Collection and processing of data

This study selected Landsat 5 (Landsat TM) images for the year 1995 and LANDSAT 8 (Operational Land Imager/ Thermal Infrared Sensor) OLS/TIRS Collection 1 Tier 1 TOA Reflectance for the year 2023. The dates were selected from January 1 to December 31.

Data for retrieving LST, NDVI, NDBI

Images were filtered according to survey data and under cloud cover of less than 2%. We applied the split window algorithm (Gislason *et alii*, 2006). In addition, all images used for LST retrieval were reflectance ratios (RR) previously corrected for atmospheric effects from Landsat 8 OLI/TIRS sensors. Figure 2 illustrates the basic steps of the research framework.

The LULC classification

A random forest model was used using a supervised classification approach (Manfothang *et alii*, 2022). Land use in the study area was then classified into four categories: metropolitan, vegetation, bare land, and forest. The urban category includes residential, commercial, and industrial areas, road infrastructure, and all impervious surfaces. The

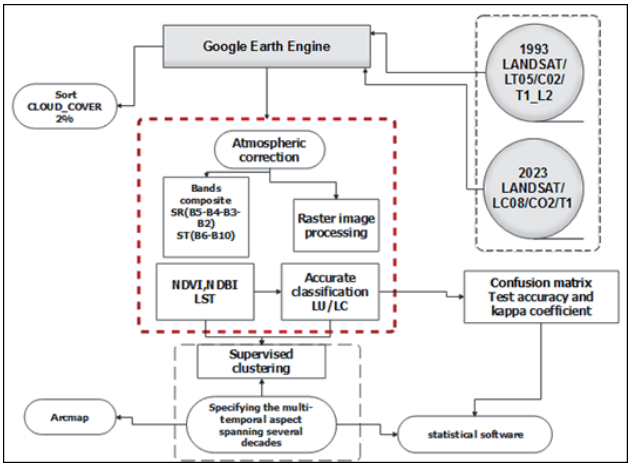

Fig. 2 - Process flowchart

vegetation category mainly contains agricultural land, wheat fields, and other areas covered with crops or grass. Conversely, bare land refers to exposed soil and areas without vegetation or buildings.

To visualize the image on the map, we embedded it as a layer by specifying specific visualization parameters, such as minimum and maximum values, and the bands used for the red, green, and blue (RGB) composition (Table 1).

LU/LC class	Course Description
Urban areas	Residential, commercial, and industrial roads, impervious surfaces
Bare lands	Sparse vegetation - undeveloped or not used for human activities - bare soil - exposed rocks.
Forest	Forest Area
Vegetation	Vegetation - Farmland, wheat fields, or similar areas covered with crops and other grasses.

Tab. 1 - Description of LU/ 2LC classes

A multi-index approach was adopted, combining NDVI, NDBI, and LST indices to gather relevant information on vegetation, agricultural land, and urban areas. Different land cover sampling points were combined into a single collection and designated as training points to create the training dataset. The training regions were generated by overlaying these points on the image stack, including all bands, and associating them with the land-cover class (Selka *et alii*, 2024). Descriptive statistics were also produced to compare the classification results with the field data collected (Rahman & Shozib, 2021). Approximately 250 samples were generated to ensure the robustness of the results (Bokaie *et alii*, 2016). To evaluate the effectiveness of the random forest model, the samples were divided into training and validation sets, with 70% of the samples used for training and the remaining 30% for validation (Parmar *et alii*, 2019).

The confusion matrix is commonly used to obtain analytical and descriptive data on classification accuracy and the Kappa coefficient (KC) to assess overall accuracy (Kraemer, 1980).

The KC (Rousta *et alii*, 2018) is expressed by equation (1):

$$\kappa = \frac{N\sum_{i=1}^{r} X_{ii} - \sum_{i=1}^{r}(X_{i+} \cdot X_{+i})}{N^2 - \sum_{i=1}^{r}(X_{i+} \cdot X_{+i})} \quad (1)$$

Where N is the total number of samples; r is the number of rows in the error matrix; X_{ii} is the total number of corrected samples in the ith row and ith column; N^2 is the square of the total number of samples; X_{i+} *is* the column total; and X_{+i} *is* the row total.

LST Recovery

For the calculation of LST, first, the raw thermal band data were converted into spectral radiance values using equation (2):

$$L_p = M_L \times Q_{Cal} + A_L \quad (2)$$

Where L_p is the top-of-atmosphere (TOA) spectral radiance (watts/(m²*sr*µm)), M_L is the multiplicative rescaling factor based on a specific band of the metadata, Q_{Cal} the quantized and calibrated pixel values (digital number (DN)) of the standard product, and A_L is the additive rescaling factor based on a specific band of the metadata (Weng *et alii*, 2004) equation (3):

$$\tau = \left[\frac{K_2}{\ln\left(\frac{K_1}{L_p} + 1\right)}\right] \quad (3)$$

Where τ is the sensor brightness temperature and K_1 and K_2 are the thermal conversion constants of the metadata.

Now, with the help of emissivity correction using equation (4), the LST (in Kelvin (K)) was derived from the brightness temperature:

$$\omega = \left[\frac{\tau}{1 + w\left(\frac{\tau}{p}\right)\ln(e)}\right] \quad (4)$$

Where ω is the sensor temperature, w is the wavelength of the emitted radiance (11.5 µm for band 6 in Landsat TM and 10.8 µm for band 10 in Landsat 8), p=h×c/s 1.438×10^{-2} mK^2, h is the Plank constant (6.626×10^{-34} Js), (Estoque *et alii*, 2018) equation (5):

$$e = nP_v + m \quad (5)$$

Where e is the emissivity of the land surface, n=0.004 and m=0.986, and P_v is the proportion of vegetation (Ranagalage *et alii*, 2017) given by equation (6):

$$Pv = \left[\frac{NDVI - NDVI_{\text{minimum}}}{NDVI_{\text{maximum}} - NDVI_{\text{minimum}}}\right]^2 \quad (6)$$

Where P_v is the proportion of vegetation and *NDVI*.

Prior to *NDVI* calculation, reflectance values were extracted from the red band and near-infrared (NIR) band using equation (7) (Choate *et alii*, 2021)

$$r_j = M_r\, Q_{cal} + A_r \quad (7)$$

Where r_j is the TOA reflectance which is devoid of solar angle correction, M_r is the multiplicative rescaling factor based on a specific band of the metadata, Q_{cal}, the quantized, and calibrated pixel values (digital number (DN)) of the standard product, and A_r the additive rescaling factor.

Finally, to obtain the value of LST in Celsius (◦C), equation (8) was incorporated (Li *et alii*, 2017):

$$LST(°C) = LST(K) - 273.15 \quad (8)$$

Calculation of NDVI

For NDVI is calculated from the reflectance values of the red band and near-infrared (NIR) band of satellite images (Aggarwal & Misra, 2018) .

It varies between −1 and +1, where high positive values indicate vegetation, low positive values indicate built-up or bare land, and negative values or values adjacent to negative values indicate water bodies. Equation (9):

$$\text{NDVI} = \frac{\text{NIR}_{\text{Band}} - \text{Red}_{\text{Band}}}{\text{NIR}_{\text{Band}} + \text{Red}_{\text{Band}}} \quad (9)$$

NIR_{Band} represents the reflectance in the near infrared band and Red_{Band} represents the reflectance in the red band.

Calculation of NDBI

The NDBI (Natural Biological Diversity Index) is used to monitor and assess built-up areas, especially in urban areas. It distinguishes built-up areas from other land use types, such as vegetation and water, and is commonly used in urban studies and land use planning (Zhang *et alii*, 2009). Its index ranges from −1 to 1, where a significant positive value denotes built-up area, a small positive value denotes bare soil, and a negative value denotes water bodies and vegetation (Varshney, 2013).

The standard NDBI formula is expressed as follows (equation 10):

$$\text{Index} = \frac{R_{\text{NIR}} - R_{\text{SWIR}}}{R_{\text{NIR}} + R_{\text{SWIR}}} \quad (10)$$

Where R_{NIR} is the reflectance in the near infrared band (band 6) and R_{SWIR} is the reflectance in the shortwave infrared band (band 5).

Correlation between indices

For each land cover type in 1993 and 2023, several key statistical parameters, such as mean, maximum, standard deviation and range were compared. In addition, since NDBI and NDVI reflect built-up and vegetated areas, respectively, a pixel-based Pearson correlation analysis was performed and developed in Python to examine the relationship between NDBI, NDVI, and LST. Pixel-based correlation analysis used LST, NDBI, and NDVI pixel values to perform Pearson analysis based on equation (11):

$$r = \frac{\sum(x-\bar{x})(y-\bar{y})}{\sqrt{\sum(x-\bar{x})^2}\sqrt{\sum(y-\bar{y})^2}} \qquad (11)$$

The r correlation coefficient was calculated by considering the value of each pixel, the average value of all pixels in each raster, and the raster image for all pixels. Furthermore, N is the number of pairs of raster images.

RESULTS

LU/LC Accuracy Evaluation Report Classification

User and producer accuracy was above 85% across all LU/LC classes, and overall accuracy achieved across all classifications was above 90%.

The Kappa coefficient was 0.92 in 1993 and 0.95 in 2023, suggesting robust land cover classification and good agreement between referenced and classified maps (Foody, 2002).

In the center of the municipality, on the other hand, there is a more marked transition towards urban areas, with a significant increase in urban areas, reflecting a process of increasing urbanization. The map displays an uneven distribution of various land use classes, with metropolitan areas primarily concentrated in the center and southern regions. At the same time, the north maintains a higher level of vegetation cover (Fig. 3).

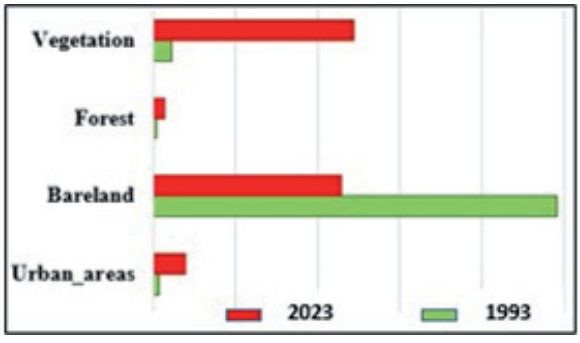

Fig. 3 - LU/LC diagram from 1993 and 2023

Spatiotemporal model of LU/LC dynamics

Land use analysis in 1993 (Fig. 4) revealed a significant predominance of bare land, representing 245.73 km² or 94% of the total area. For comparison, forests covered 11.21 km², urban areas 3.27 km² and vegetation class 1.75 km².

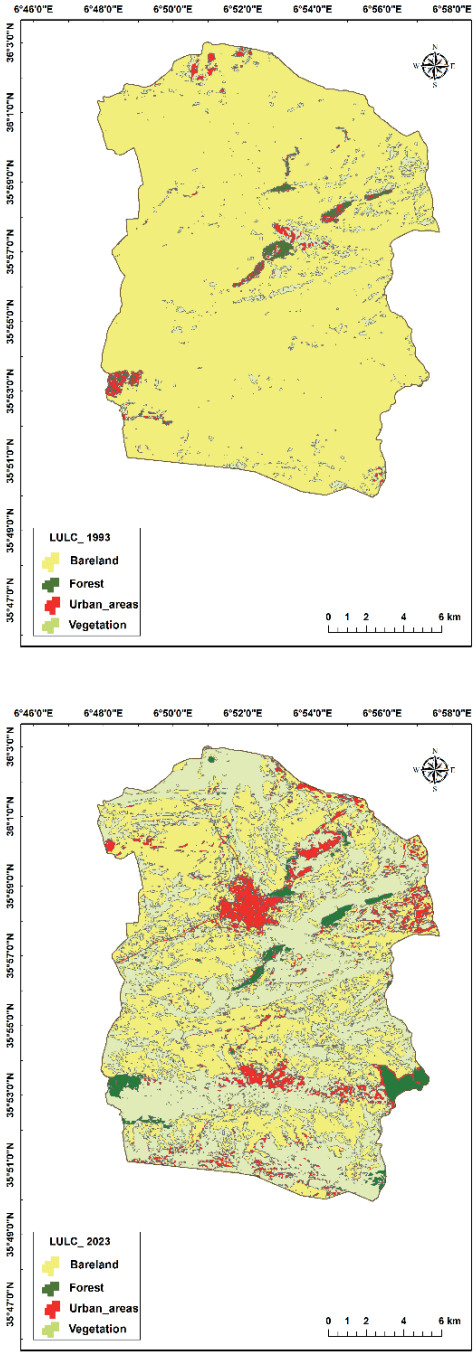

Fig. 4 - LU/LC map of Ain Fakroun in 1993 and 2023

The north of the region has a strong presence of vegetated areas and forests, indicating a relatively dense vegetation cover.

Land use changes for 2023 (Fig. 4) are significant, with a notable decrease in the area occupied by bare land, which amounts to 113.94 km², or 43% of the total area. On the other hand, the area devoted to vegetation increased, reaching 122.18 km² and representing 47% of the region. The increase in forest area also corroborates this trend.

The map also shows an expansion of urban areas, particularly in the center and south of the region. In the north, vegetation and forest cover remain high despite slight fragmentation due to urban expansion. Urbanization is more pronounced in the center, with the increase in urban areas reflecting a corresponding increase in pressure on natural resources. In the south, bare land is decreasing, while vegetation and forest areas are increasing (Fig. 4).

LST of the study area

The LST analysis revealed that the minimum and maximum temperature values were 13.53 °C and 41.54 °C, respectively. In 1993 and 2023, the minimum value was 19.45 °C, and the maximum value was 46.66 °C. There has been a general increase in LST over 30 years, indicating an overall warming of the region. In 1993, temperatures were lower in the north and higher in the south; in 2023, the distribution of higher temperatures was uniform and dominant.

The colder areas of 1993 were reduced after 30 years, indicating significant climate warming in this region. (Fig. 5).

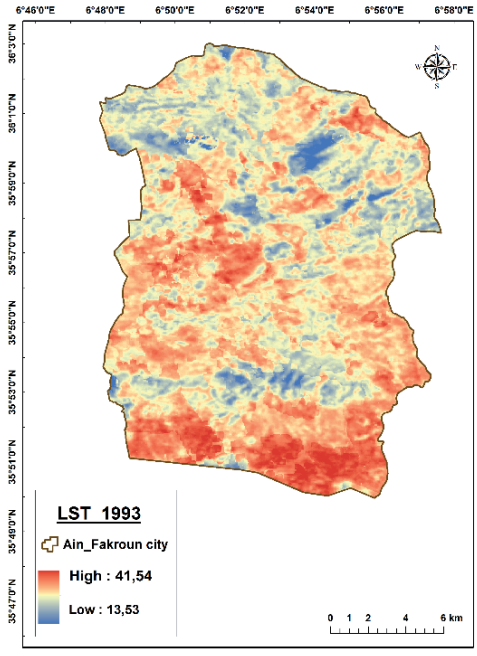

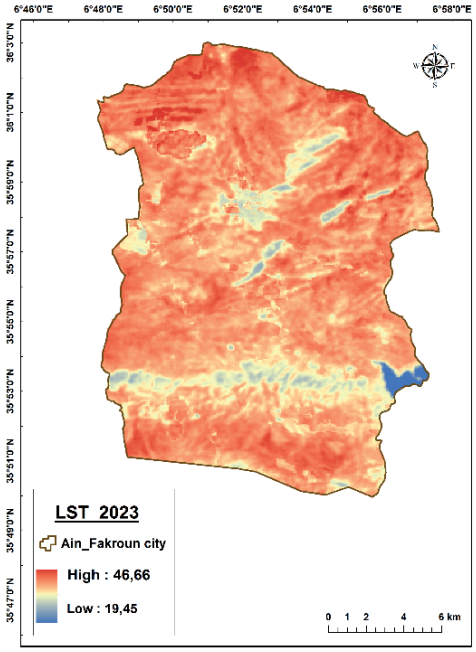

Fig. 5 - LST map of Ain Fakroun in 1993 and 2023

Relationship between LU/LC and LST

Average LST values were calculated for each class (urban, bare land, forest, and vegetation) (Weng *et alii*, 2004) (Fig. 6). With an increase of almost 2% for urban areas, indicating expansion over 30 years, and a slight increase for bare land and forest areas, with a slight increase (0.5% and 1.5%, respectively). For vegetation areas, there was a reduction of 1.5%, from 34.73 to 33.23 (Fig. 7).

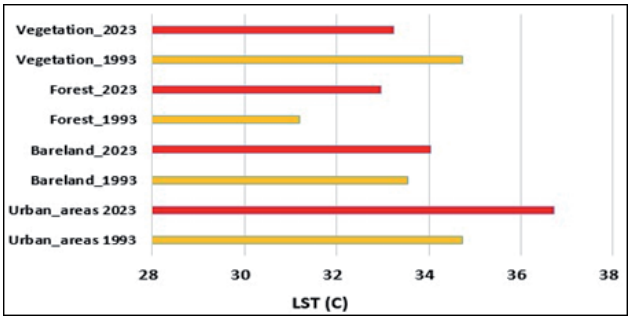

Fig. 6 - Diagram LST of 1993 and 2023

These data indicate a trend toward urbanization, characterized by an increase in urban areas and a slight expansion of bare land. With reforestation operations, forest areas have also increased.

These changes suggest a transformation of the landscape, driven by urban growth, and a possible shift in priority towards the preservation or expansion of forests. To better understand these changes, it would be beneficial to have more context on the region in question and its land use policies.

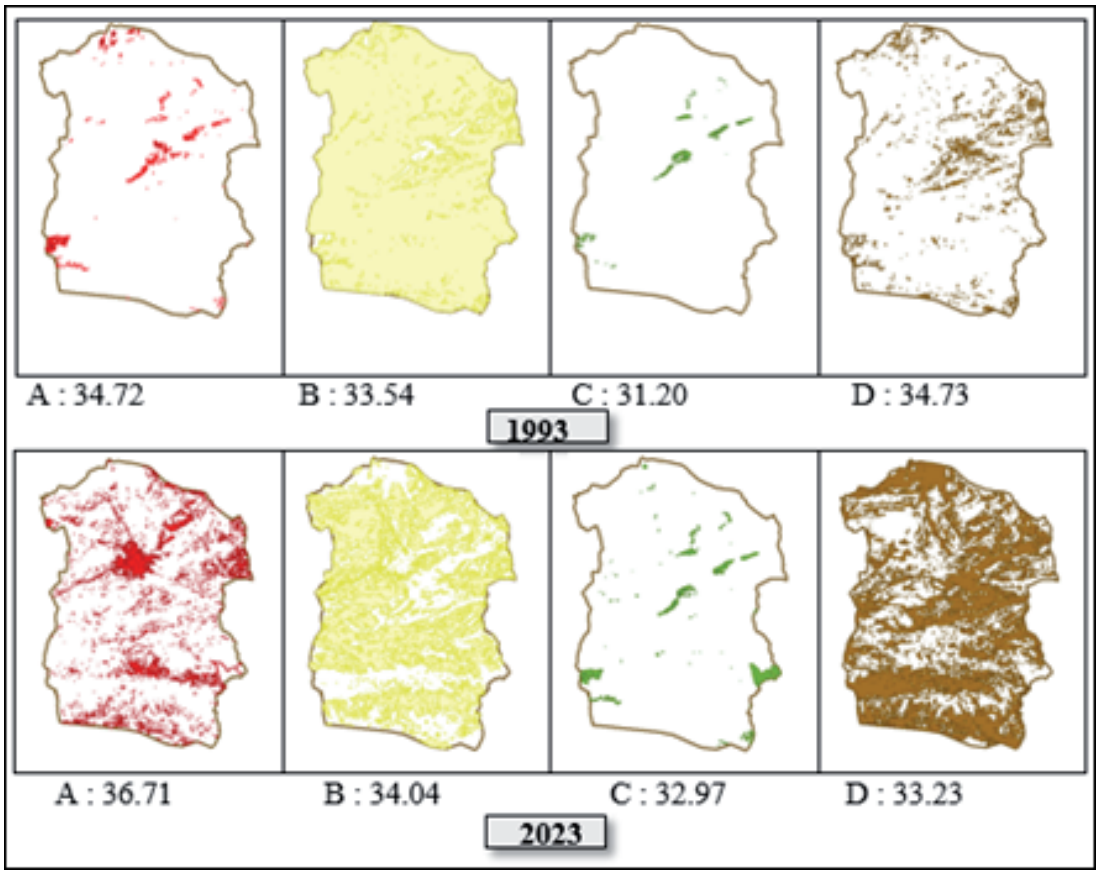

Fig. 7 - LU/LC from 1993 and 2023 (A: Urban area, B: Bareland, C: Forest, D::Vegetation)

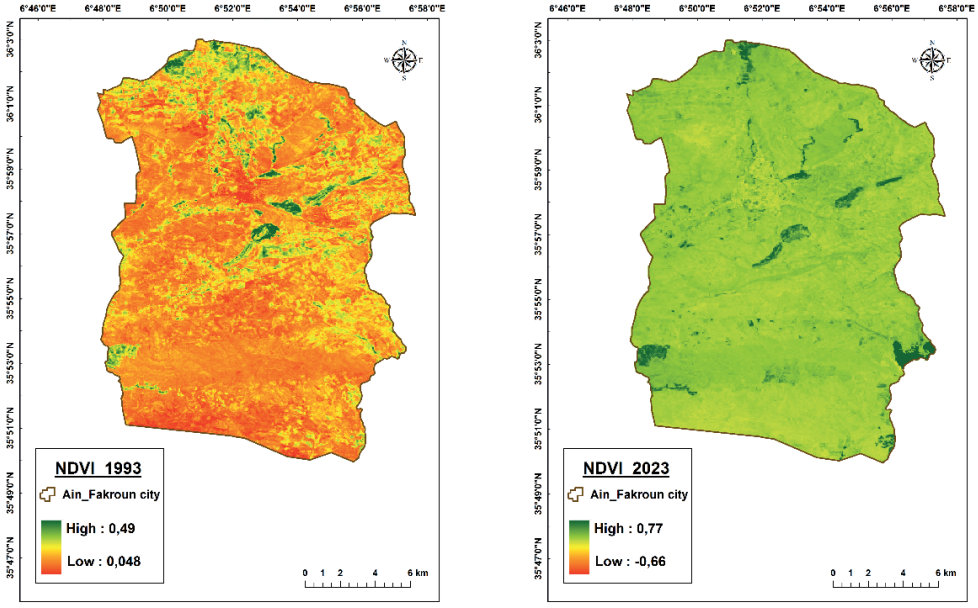

Fig. 8 - NDVI map of Ain Fakroun in 1993 and 2023

NDVI map and relationship with LST

Data analysis reveals a persistent inverse relationship between vegetation index (NDVI) and surface temperature (LST). In 1993, this relationship was more pronounced, with high NDVI associated with low LST (30-32°C) and low NDVI (0.10-0.13) related to high LST (37-39°C). Figure 8 shows that by 2023, the peak NDVI has increased from 0.49 to 0.77 and decreased from 0.04 to -0.16, indicating an overall increase in vegetation, including agricultural areas, which is a significant factor in NDVI variations. At the same time, the distribution of TPS has shifted from a concentration around 32-34°C in 1993 to a more uniform distribution between 32°C and 40°C in 2023. (Figs. 6 and 9). Although the inverse NDVI-LST relationship persists in 2023 (Fig. 9), it appears less pronounced, underlining the impact of land-use changes on the local microclimate and the crucial importance of vegetation in urban thermal regulation. (Fig. 8)

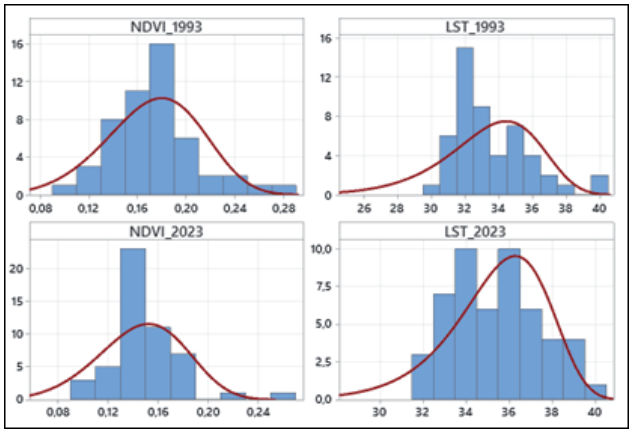

Fig. 9 - Diagonal matrix plot of NDVI_1993; LST_1993; NDVI_2023; LST_2023

NDBI Card and Relationship with LST

There is a positive correlation between the NDBI index and the LST, both in 1993 and 2023. There is a general trend of increasing LST as the NDBI increases.

In 1993, the NDBI distribution peaks around 0.05, while the LST is mainly concentrated between 30 °C and 35 °C. In 2023, the NDBI distribution shifts towards higher values, peaking around 0.1, accompanied by dispersion and a slight increase in LST, which now extends up to 40 °C.

This change is attributed to the intensification of urbanization between 1993 and 2023, characterized by an increase in built-up areas (higher NDBI) and a corresponding rise in surface temperatures (Fig. 10). The positive correlation between NDBI and LST is explained by the ability of urban surfaces to absorb and retain heat, thus contributing to the urban heat island effect. Urban materials, such as asphalt and concrete, tend to store heat during the day and release it slowly, resulting in higher temperatures in urban areas compared to surrounding rural areas (Fig. 10).

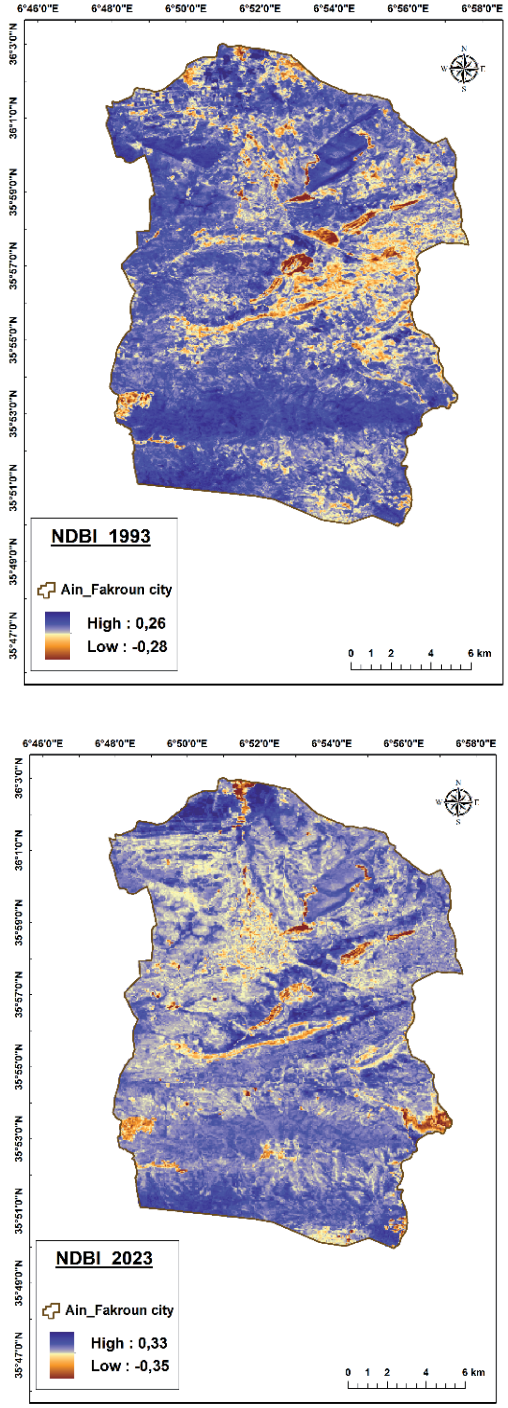

Fig. 10 - NDBI map of Ain Fakroun in 1993 and 2023

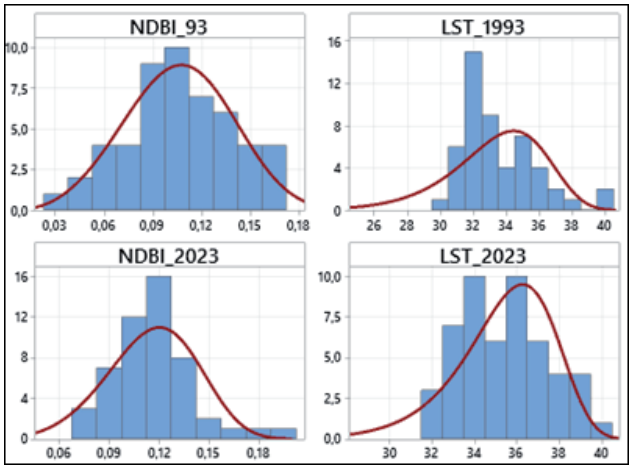

Fig. 11 - Diagonal matrix plot of NDBI_1993; LST_1993; NDVI_2023; LST_2023

DISCUSSIONS

Urban development: a change in housing and the city and its intensification on the LST

The city has experienced rapid, impermeable development in the form of residential, commercial, transportation, and parking networks, among others. This LU/LC dynamic has changed the scenario of large-scale LST distribution (Dos Santos *et alii*, 2017).

The explosive population growth of the last 30 years is one of the primary drivers of this transformation, with the population increasing from approximately 45000 inhabitants in 1993 to around 70000 inhabitants in 2023. This demographic surge has significantly stimulated housing demand, resulting in the launch of numerous significant real estate projects. These initiatives include programs led by the National Agency for Housing Improvement and Development (AADL), participatory social housing (LSP), and the ambitious one million social housing program, mainly concentrated in the northwestern part of the study area. These results are consistent with those reported in the Tlemcen region (Selka *et alii*, 2024).

A similar type of transformation has been observed due to the rapid development of built-up areas in different parts of the world, such as in Baguio City in the Philippines (Estoque & Murayama, 2017), Istanbul City in Turkey (Nigussie & Altunkaynak, 2017) and Mekelle City in Ethiopia (Fenta *et alii*, 2017). This study (Ghaderpour *et alii*, 2024) uses MODIS LST and land cover data from 2000 to 2023 to analyze spatiotemporal surface temperature changes in Central Italy, revealing nighttime warming trends linked to vegetation expansion, elevation effects, and implications for wildfire and landslide risk management.

Our study revealed a significant increase in temperatures across all categories, with drylands experiencing the highest annual temperatures. This trend is attributed to their low thermal inertia and low evapotranspiration, a consequence of the absence of vegetation. Correlations between indices confirm these results (Table 2).

Sample 1	Sample 2	N	Correlation	IC - 95% for ρ	P Value
NDBI_93	NDVI_93	51	-0,682	(-0,817 ; -0,477)	0,000
LST_93	NDVI_93	51	-0,426	(-0,635 ; -0,158)	0,002
LST_93	NDBI_93	51	0,278	(-0,003 ; 0,518)	0,048

Tab. 2 - Correlation between indices two by two in 1993

A comparison of the correlations between NDVI, NDBI, and LST indices from 1993 to 2023 reveals significant changes. In 1993, the correlation between NDVI and NDBI was strongly negative (-0.682), indicating that an increase in vegetation was strongly associated with a decrease in built-up areas (Malik *et alii*, 2019). Furthermore, the moderate negative correlation between NDVI and LST (-0.426) suggested that more vegetation was associated with lower surface temperatures. In contrast, the weaker positive correlation between NDBI and LST (0.278) reflected an association between more built-up areas and higher surface temperatures. By 2023, the relationship between NDVI and NDBI had shifted to a weaker negative correlation, indicating a reduced impact of vegetation on built-up areas (Table 3).

Sample 1	Sample 2	N	Correlation	IC - 95% for ρ	P Value
NDBI_2023	NDVI_2023	51	-0,215	(-0,466 ; 0,067)	0,129
LST_2023	NDVI_2023	51	-0,043	(-0,315 ; 0,236)	0,765
LST_2023	NDBI_2023	51	0,061	(-0,218 ; 0,331)	0,670

Tab. 3 - Correlation between indices two by two in 2023

This discrepancy suggests that the vegetated areas identified in the images were primarily agricultural land characterized by sparse vegetation suitable for wheat cultivation, as this region is known for producing high-quality wheat and other similar crop varieties. This mainly involves the transition from a system dominated by pastoralism, based on livestock, transhumance, and pastures, to an agricultural system characterized by irrigated crops.

Areas classified as bare land exhibit temperatures that vary depending on the soil type (clay, sand, or peat) and external factors, such as ambient temperature (Bokaie *et alii*, 2016).

According to the results of various studies, a negative correlation was found between vegetation and surface temperature, which can be explained by the reduction of vegetation cover and its conversion to mineral surfaces (Zhang *et alii*, 2009).

One of the striking observations of this article concerns the evolution of the average surface temperature (MST) in the urbanization of the city of Aïn Fakroun. In the city center, the average surface temperature was systematically lower than that of the peripheral areas (Fig. 11); this gap is particularly marked in 2023. The MST increased due to a rise in the NDBI, linked to

intense demographic pressure that has intensified mainly over the last thirty years.

This is consistent with the results of other studies conducted in Barcelona and Rotterdam (Van Hove *et alii*, 2015).

LST, NDVI, and NDBI Association

The relationship between NDVI and LST has been widely studied in various cities around the world, including Shanghai, China (Yue *et alii*, 2007), and Mashhad, Iran (Fatemi & Narangifard, 2019), with results showing a negative correlation between these indices.

The positive association between LST and NDBI detected in the current research is consistent with most previous studies (Fatemi & Narangifard, 2019). This association demonstrates that both built-up areas and bare land directly affect high LST values. Some studies, such as those by Feng *et alii* (Fatemi & Narangifard, 2019) and Guha *et alii* (Guha *et alii*, 2020), demonstrate that the NDBI and LST association is influenced by land cover types and seasonal changes, similar to the NDVI and LST association. One of the main reasons for the inverse association between NDBI and LST is the expansion of the city, which has reduced the LST value (towards the periphery) (Azhdari *et alii*, 2018). In the case of Ain Fakroun, the city center, as well as the eastern and southwestern suburbs, showed a negligible positive relationship between NDBI and LST.

This result is consistent with the results of previous studies (Azhdari *et alii*, 2018).

Advantages and limitations of the current study

Google Earth Engine provides a powerful platform for geospatial analysis, enabling the processing of large volumes of cloud-based satellite data without the need for local download.

This tool is handy for multi-temporal studies on the evolution of urban, agricultural, or natural areas. However, its use is limited by certain technical constraints.

Users may encounter difficulties related to computational time, particularly when analyzing large areas or running complex algorithms, which can slow down the generation of results. Memory overruns ("user memory limit exceeded") are also a standard limitation, especially when scripts incorporate intensive operations or long time series. Finally, restrictions on export file sizes sometimes make it difficult to extract detailed results, leading to split analyses or reduced spatial resolution.

Furthermore, this study relied on Landsat images from the years 1984 and 2023, which presents a notable limitation: the absence of intermediate data in this region does not allow for the analysis of annual trends or seasonal fluctuations over the 30 years. This gap also prevents the study of interannual cycles and more precise evolutionary dynamics, which could be considered in future work.

CONCLUSIONS

Accurate and long-term land-use/land-cover (LULC) data play a crucial role in the sustainable management of natural resources in Algeria's semi-arid regions.

In the present study, we began by analyzing the LULC changes in Ain Fakroun city for the years 1993 and 2023, covering the period from January 1 to December 31, using the Random Forest (RF) algorithm on the Google Earth Engine platform, as well as Landsat 5 and 8 images. Change detection analysis enabled us to compare the patterns of spatiotemporal land-use/land-cover (LULC) changes. The convenience of the approach used can be considered in the future as a reference for conducting studies similar in other regions.

The main results reveal a marked increase in urban areas, vegetation, and land area. However, this urban growth has exacerbated the Urban Heat Island (UHI) effect, as evidenced by the increase in Land Surface Temperature (LST) values across all categories of land use.

The study also identifies the technical challenges related to the use of GEE, such as computational constraints and file size limitations, but highlights its potential for scalable environmental monitoring.

The results provide actionable information for decision-makers, policymakers, and urban planners, advocating for sustainable development through the integration of green infrastructure, preservation of natural ecosystems, and adoption of high albedo materials to mitigate the effects of UHI and strengthen resilience to climate change. In conclusion, this research contributes to the understanding of the interaction between urbanization, vegetation, and built-up areas.

ACKNOWLEDGMENTS

We would like to express our sincere gratitude to the Google Earth Engine platform for providing an exceptional environment for geospatial analysis and to the DGRST of Algeria.

REFERENCES

Aggarwal S. & Misra M. (2018) - *Comparaison des indices NDVI et NDBI comme indicateurs des effets d'îlot de chaleur de surface à Bangalore et New Delhi : étude de cas*. Technologies de télédétection et applications en milieu urbain III, **10793**: 178-186. https://doi.org/10.1117/12.2325738.

Avdan U. & Jovanovska G. (2016) - *Algorithme de cartographie automatisée de la température de surface terrestre à partir des données satellitaires LANDSAT 8.* Journal of Sensors, **1**: 1480307. https://doi.org/10.1155/2016/1480307.

Azhdari A., Soltani A. & Alidadi M. (2018) - *Effet de la morphologie urbaine et de la structure du paysage sur la température de la surface terrestre: données de Shiraz, une ville semi-aride.* Villes et société durables, **41**: 853-864.

Benoumeldjadj M., Rached-kanouni M. & Bouchareb A. (2024) - *Évaluation de la vulnérabilité agricole à la sécheresse à l'aide de l'indice de santé de la végétation: étude de cas à Constantine.* Résumé, **93**(1): 32-49. https://journal.ugm.ac.id/ijg/issue/view/5213.

Bokaie M., Zarkesh M.K., Arasteh P.D. & Hosseini, A. (2016). - *Évaluation de l'îlot de chaleur urbain basée sur la relation entre la température de surface et l'occupation du sol à Téhéran.* Villes et société durables, **23**: 94-104.

Budhwar P., Chowdhury S., Wood G., Aguinis H., Bamber G.J., Beltran J.R., Boselie P., Lee Cooke F., Decker S. & De Nisi A. (2023) - *La gestion des ressources humaines à l'ère de l'intelligence artificielle générative : perspectives et orientations de recherche sur ChatGPT.* Revue de gestion des ressources humaines, **33**(3): 606-659.

Dos Santos A.R., De Oliveira F.S., Da Silva A.G., Gleriani J.M., Gonçalves W., Moreira G.L., Silva F.G., Branco E.R.F., Moura M.M. & Da Silva R.G. (2017) - *Répartition spatiale et temporelle des îlots de chaleur urbains.* Science de l'environnement total, **605**: 946-956.

Estoque R.C. & Murayama Y. (2017) - *Surveillance de la formation d'îlots de chaleur urbains de surface dans une ville tropicale de montagne à l'aide de données Landsat (1987-2015).* Revue de photogrammétrie et de télédétection de l'ISPRS, **133**:18-29.

Fatemi M. & Narangifard M. (2019) - *Suivi des variations de la consommation d'énergie et de son impact sur le LST et le NDVI dans le district 1 de la ville de Shiraz.* Arabian Journal of Geosciences, **12**(4): 127.

Fenta A.A., Yasuda H., Haregeweyn N., Belay A.S., Hadush Z., Gebremedhin M.A. & Mekonnen G. (2017) - *La dynamique de l'expansion urbaine et les changements d'utilisation et de couverture des sols grâce à la télédétection et aux mesures spatiales: le cas de la ville de Mekele, dans le nord de l'Éthiopie.* Revue internationale de télédétection, **38**(14): 4107-4129.

Foody G.M. (2002) - *État de l'évaluation de la précision de la classification de la couverture terrestre.* Télédétection de l'environnement, **80**(1): 185-201.

Ghaderpour E., Mazzanti P., Bozzano F., Scarascia Mugnozza G. (2024) - *Trend analysis of MODIS land surface temperature and land cover in central Italy.* Land. **13**(6): 796. https://doi.org/10.3390/land13060796.

Gislason P.O., Benediktsson J.A. & Sveinsson J.R. (2006) - *Forêts aléatoires pour la classification de la couverture terrestre.* Pattern Recognition Letters, **27** (4): 294-300.

Gorelick N. (2013) - *Moteur Google Earth.* Résumés de la conférence de l'Assemblée générale de l'EGU, **15**:1997.

Guha S., & Govil H. (2022) - *Évaluation annuelle de la relation entre la température de la surface terrestre et six indices de télédétection utilisant les données Landsat de 1988 à 2019.* Geocarto International, **37**(15): 4292-4311.

Guha S., Govil H., Dey A., & Gill N. (2020) - *Étude de cas sur la relation entre la température de surface terrestre et les indices de surface terrestre dans la ville de Raipur, en Inde.* Géographie - Revue danoise de géographie, **120**(1): 35-50.

Kraemer H.C. (1980) - *Extension du coefficient kappa.* Biométrie, 207-216.

Kumar D. & Shekhar S. (2015) - *Analyse statistique de la relation entre la température de surface terrestre et les indices de végétation par télédétection thermique.* Écotoxicologie et sécurité environnementale, **121**: 39-44.

Mahcer I., Baahmed D., Chemirik C.H.K. & Nedjai R. (2024) - *Cartographie des impacts environnementaux dans le nord-ouest de l'Algérie par analyse spatio-temporelle multivariée utilisant la télédétection et le système d'information géographique.* Ingénierie écologique et technologie environnementale (EEET), **25**(5).

Malik M.S, Shukla J.P & Mishra S. (2019) - *Relation entre LST, NDBI et NDVI à l'aide des données Landsat-8 dans le bassin versant de Kandaihimmat, Hoshangabad, Inde* . Indian Journal of Geo-Marine Geosciences, **48**(1): 25-31.

Manfothang E.D., Tumenta P., Tassiamba S.N., Nguimdo V.R. & Defouh K.Y. (2022) - *Diversité Floristique et Structure des Peuplements de la Forêt Communale de Ngambe-Ndom-Nyanon, Région du Littoral du Cameroun.* Journal ouvert de foresterie, **12**(4): 503-520.

Marzban F., Sodoudi S. & Preusker R. (2018) - *Influence du type de couverture terrestre sur la relation entre le NDVI–LST et le LST-T de l'air.* Revue internationale de télédétection, **39**(5): 1377-1398.

Nigussie T.A. & Altunkaynak A. (2017) - *Modélisation de l'urbanisation d'Istanbul selon différents scénarios à l'aide du modèle de croissance urbaine SLEUTH.* Journal of Urban Planning and Development, **143**(2): 4016037.

Parmar A., Katariya R. & Patel V. (2019) - *Une revue de la forêt aléatoire: un classificateur d'ensemble.* Conférence internationale sur les technologies intelligentes de communication de données et l'Internet des objets (ICICI) 2018, 758-763.

Patel S., Indraganti M. & Jawarneh R.N. (2023) - *Revue systématique complète : Impact de l'utilisation et de la couverture terrestres (UTC) sur les températures de surface terrestres (TST) et le confort thermique extérieur.* Bâtiment et environnement, 111130.

Paz - Ferreiro J. & Fu S. (2016) - *Indices biologiques pour l'évaluation de la qualité des sols: perspectives et limites.* Dégradation des terres et développement, **27**(1): 14-25.

Rahman M.N. & Shozib S.H. (2021) - *Variabilité saisonnière de l'engorgement dans la municipalité de Rangpur à l'aide de techniques SIG et de télédétection.* Geosfera Indonesia, **6**(2): 143-156.

Ranagalage M., Estoque R.C., Zhang X. & Murayama Y. (2018) - *Évolution spatiale de la formation d'îlots de chaleur urbains dans le district de Colombo, au Sri Lanka : implications pour la planification durable.* Sustainability, **10**(5): 1367.

Selka I., Mokhtari A.M., Tabet Aoul K.A., Bengusmia D., Malika K. & Djebbar K.E.B. (2024) - *Évaluation de l'impact des changements d'occupation et d'utilisation des sols sur la dynamique des températures de surface à l'aide de Google Earth Engine : étude de cas de la municipalité de Tlemcen, dans le nord-ouest de l'Algérie (1989-2019).* Revue internationale de géo-information de l'ISPRS, **13**(7). https://doi.org/10.3390/ijgi13070237.

Singh S.K., Mustak S., Srivastava P.K., Szabó S. & Islam T. (2015) - *Prévision des variations spatiales et décennales de la consommation d'énergie (LULC) grâce à des modèles de chaînes de Markov à automates cellulaires utilisant des ensembles de données d'observation de la Terre et des géoinformations.* Environmental Processes, **2**: 61-78.

Sultan B. (2011) - *L'étude des variations et du changement climatique en Afrique de l'Ouest et ses retombées sociétales.* Habilitation à Diriger Des Recherches, Université Pierre et Marie Curie .

Van Hove L.W.A., Jacobs C.M.J., Heusinkveld B.G., Elbers J.A., Van Driel B.L. & Holtslag A.A.M. (2015) - *Variabilité temporelle et spatiale de l'îlot de chaleur urbain et du confort thermique dans l'agglomération de Rotterdam.* Bâtiment et environnement, **83**: 91-103.

Varshney A. (2013) - *Amélioration de l'algorithme de différenciation NDBI pour la détection des changements dans les zones bâties à partir de données de télédétection: une approche automatisée.* Remote Sensing Letters, **4**(5): 504-512.

Vinh N.Q., Khanh N.T. & Anh P.T. (2020) - *Interrelations entre lst, ndvi et ndbi en télédétection pour la résilience à la sécheresse à Ninh Thuan, Vietnam.* ICSCEA 2019, Actes de la Conférence internationale sur le génie civil et l'architecture durables, 201-209.

Weng Q., Lu D. & Schubring J. (2004) - *Estimation de la relation entre la température de surface terrestre et l'abondance de la végétation pour les études sur les îlots de chaleur urbains.* Télédétection environnementale, **89**(4): 467-483. https://doi.org/10.1016/j.rse.2003.11.005.

Yue W., Xu J., Tan W. & Xu L. (2007) - *Relation entre la température de surface terrestre et l'indice NDVI avec la télédétection: application aux données ETM+ du satellite Landsat 7 de Shanghai.* Revue internationale de télédétection, **28**(15): 3205-3226.

Zellweger F., De Frenne P., Lenoir J., Rocchini D. & Coomes D. (2019) - *Progrès en écologie du microclimat grâce à la télédétection.* Tendances en écologie et évolution, **34**(4): 327-341.

Zeren Cetin I., Varol T., Ozel H.B. & Sevik H. (2023) - *Les effets du climat sur l'utilisation et la couverture des terres: une étude de cas en Turquie utilisant des données de télédétection.* Environmental Science and Pollution Research, **30**(3): 5688-5699.

Zhang Y., Odeh I.O.A. & Han C. (2009) - *Caractérisation bitemporelle de la température de surface terrestre en fonction de la surface imperméable, NDVI et NDBI, à l'aide d'une analyse d'images sous-pixel.* Revue internationale d'observation appliquée de la Terre et de géoinformation, **11**(4): 256-264. https://doi.org/10.1016/j.jag.2009.03.001.

Received April 2025 - Accepted June 2025